Title
Sprouting angiogenesis induces significant mechanical heterogeneities and ECM stiffening across length scales in fibrin hydrogels

Authors
Juliar, Benjamin A
Keating, Mark T
Kong, Yen P
et al.

Publication Date
2018-04-01

DOI
10.1016/j.biomaterials.2018.02.012

Peer reviewed

HHS Public Access

Author manuscript

Biomaterials. Author manuscript; available in PMC 2019 April 01.

Published in final edited form as:

Biomaterials. 2018 April ; 162: 99–108. doi:10.1016/j.biomaterials.2018.02.012.

Sprouting angiogenesis induces significant mechanical heterogeneities and ECM stiffening across length scales in fibrin hydrogels

Benjamin A. Juliar[1,*], **Mark T. Keating**[2,*], **Yen P. Kong**[1], **Elliot L. Botvinick**[2,+], and **Andrew J. Putnam**[1,+]

[1]Department of Biomedical Engineering, University of Michigan; Ann Arbor, Michigan

[2]Department of Biomedical Engineering, University of California, Irvine; Irvine, California

Abstract

Matrix stiffness is a well-established instructive cue in two-dimensional cell cultures. Its roles in morphogenesis in 3-dimensional (3D) cultures, and the converse effects of cells on the mechanics of their surrounding microenvironment, have been more elusive given the absence of suitable methods to quantify stiffness on a length-scale relevant for individual cell-extracellular matrix (ECM) interactions. In this study, we applied traditional bulk rheology and laser tweezers-based active microrheology to probe mechanics across length scales during the complex multicellular process of capillary morphogenesis in 3D, and further characterized the relative contributions of neovessels and supportive stromal cells to dynamic changes in stiffness over time. Our data show local ECM stiffness was highly heterogeneous around sprouting capillaries, and the variation progressively increased with time. Both endothelial cells and stromal support cells progressively stiffened the ECM, with the changes in bulk properties dominated by the latter. Interestingly, regions with high micro-stiffness did not necessarily correlate with remodeled regions of high ECM density as shown by confocal reflectance microscopy. Collectively, these findings, especially the large spatiotemporal variations in local stiffness around cells during morphogenesis in soft 3D

[+]Corresponding authors: Elliot L. Botvinick, Ph.D., Department of Biomedical Engineering, University of California, Irvine, 2416 Engineering Hall, Irvine, CA 92697-2730, Phone: (949) 824-9613, Fax: (949) 824-8413, elliot.botvinick@uci.edu. Andrew J. Putnam, Ph.D., Department of Biomedical Engineering, University of Michigan, 2204 Lurie Biomedical Engineering Building, 1101 Beal Ave, Ann Arbor, MI 48109, Phone: (734) 615-1398, Fax: (734) 647-4834, putnam@umich.edu.

[*]BAJ and MTK are co-first authors

[+]ELB and AJP are co-corresponding authors

Author Contributions:

E.B. and A.P. conceived the ideas, provided the resources, and managed the entire project. All authors contributed to experimental design, and discussed/interpreted results. B.J. performed quantitative sprouting angiogenesis assays (and essential controls) and applied bulk rheological measurements as a function of time. M.K. performed additional sprouting angiogenesis assays (and controls), and applied AMR and confocal reflection methods as a function of time. Y.K. developed the bulk rheological methods and assisted B.J. in their application. B.J. and M.K. analyzed the data, performed statistical comparisons, and prepared all the figures. All authors contributed text for early drafts of the manuscript, with B.J. and A.P. performing the editing and revising to attain the final version. All authors read and approved the final version of the paper.

Data Availability Statement:

All data required to reproduce these findings are available from the corresponding authors upon request.

fibrin gels, underscore that characterizing ECM mechanics across length scales provides an opportunity to attain a deeper mechanobiological understanding of the microenvironment's roles in cell fate and tissue patterning.

Keywords

Endothelial cells; fibroblasts; microrheology; optical tweezers; fibrin; microvasculature

Introduction

Numerous cell types demonstrate differential phenotypic responses and differentiation potential depending on the elasticity of the environment in which they reside [1]. Tuning substrate rigidity in 2D, ostensibly without altering porosity, diffusive transport, or ligand density, alters cell spreading [2, 3], proliferation [4, 5], migration [3, 6], and differentiation [7, 8]. Despite the interdependence of elasticity with other properties in real tissues, ECM mechanical properties also appear to control cell fate in 3D [9, 10]. Nevertheless, despite considerable interest in the effects of matrix rigidity on cell phenotypes, how cells change the mechanical properties of the surrounding ECM, particularly on a microscale, remains poorly understood. Moreover, the instructive cue of matrix stiffness has largely been treated as unidirectional and static, with measurements of bulk stiffness at a singular initial time point correlated with cell fate. In reality, complex morphogenetic processes in 3D involve dynamic and reciprocal mechanical cross-talk between cells and the surrounding ECM.

ECM stiffness has also been postulated to be an important instructive cue governing capillary morphogenesis [11], affecting the magnitudes of contractile forces endothelial cells (ECs) exert on their surroundings to control their invasive abilities [12]. We have previously shown that EC contractile forces are essential for capillary morphogenesis [13], and the rate at which ECs deform ECM fibers depends on the initial matrix concentration and correlates with the rate at which they form vessel-like structures in 3D [14]. However, different material platforms and cross-linking schemes have led to discrepancies in the literature, with some studies suggesting softer matrices are more supportive of vascular morphogenesis and others reporting higher stiffness yields more invasion. Regardless, across all material platforms, the spatiotemporal evolution of ECM micromechanics during angiogenic sprouting remains unclear.

In this study, we exploited a well characterized model of angiogenic sprouting in which ECs coated on microcarrier beads invade a 3D fibrin matrix when co-cultured with stromal fibroblasts [15, 16]. Fibrin is the major component of the provisional matrix in a blood clot [17], and thus is a suitable model for investigating the mechanical evolution of ECM during wound healing. Fibroblasts secrete pro-angiogenic cytokines and other factors that are essential for EC tubulogenesis when co-embedded with ECs in the fibrin matrix, where they can act in a pericyte-like manner and directly associate with the nascent capillaries [18], or overlaid on top of the gels as a monolayer [19, 20]. In addition to supporting angiogenesis, fibroblasts play important roles in wound closure and healing by increasing contractility and depositing ECM [21], both of which effect the elasticity of the matrix [20, 22].

Through a combination of shear rheology to track bulk elastic properties and laser-based optical tweezers active microrheology (AMR) to quantify elasticity on a length scale relevant for individual cells, we explicitly quantified changes in ECM mechanics across length scales, over time, and with unprecedented resolution during the complex morphogenetic process of angiogenic sprouting *in vitro*. Our findings reveal significant mechanical heterogeneities encountered by cells on the microscale, and demonstrate the extent to which the ECs themselves alter the mechanical properties of the surrounding ECM. We further assessed whether pericytic association affects the rate and degree to which local ECM stiffening occurs, and determined the effect fibroblasts have on the ECM when distant from sprouting microvasculature. Collectively, this study highlights the importance of characterizing ECM mechanical properties on an appropriate length scale and over time, as initial bulk characterization misses the dynamic and highly varied environment individual cells experience.

Materials and Methods

Cell culture

Normal human dermal fibroblasts (DFs, Lonza, Walkersville, MD) were cultured in Dulbecco's modified eagle medium (DMEM, Life Technologies, Grand Island, NY) supplemented with 10% fetal bovine serum (FBS, Life Technologies) and 1% penicillin streptomycin (Life Technologies) and were used up to passage 7. Human umbilical vein endothelial cells (ECs) were either harvested from fresh umbilical cords as previously described [15] or purchased from a commercial source (Lonza). Two different sources of ECs were used to ensure robustness of the observed biological responses. The ability of these two different sources of HUVECs to sprout in our fibrin-based assays was quantitatively equivalent (data not shown). HUVECs for all experiments were cultured in fully supplemented EGM2 (Lonza) and used between passages 2–4. Media for both cell types were exchanged 3 times a week and cells were harvested below 80% confluence using 0.05% trypsin-EDTA (Life Technologies).

Fibrin-based capillary morphogenesis assay

A three-dimensional cell culture model of capillary morphogenesis was assembled following adapted protocols as previously described [15, 16, 23]. Briefly, EC-coated microbeads were embedded in fibrin gels with DFs either embedded or overlaid on the gel as a monolayer. A stock solution of sterilized Cytodex microcarrier beads (Sigma-Aldrich, St Louis, MO) was prepared ahead of time by autoclaving in PBS. The day before construct assembly, microbeads were coated with ECs by combining 1×10^4 microbeads with 4×10^6 ECs in 5 mL of EGM2 in an upright T-25 tissue culture flask (Corning Inc, Corning, NY). The flask was incubated for 4 hours with periodic agitation every 30 minutes. Afterwards, 5 mL of fresh EGM2 was added, and the 10 mL suspension of freshly coated beads was transferred to a new T-25 and allowed to incubate overnight in the standard tissue culture position. The following day, beads were transferred to a 15 mL conical tube (VWR, Radnor, PA) and allowed to settle by gravity between two washes with fresh EGM2. Fibrinogen from bovine plasma (Sigma) was dissolved in serum free EGM2 to achieve a final concentration of 2.5 mg/mL clottable fibrinogen upon gelation, and sterile filtered through a 0.22 μm PES

membrane filter (Merck Millipore Ltd, Tullagreen, Carrigtwohill, Co. Cork, IRL). For conditions in which the stromal fibroblasts were embedded within the fibrin gel ("embedded") a suspension of DFs was added to the fibrinogen at a final concentration of 2.5×10^4 cells/mL; for the other conditions, an equal volume of EGM2 was added instead. Microbeads were added to the solution at 50 beads/mL. Heat-inactivated FBS was added to the solution immediately prior to gelation for a final concentration of 5%. Tissue culture dishes were spotted with 40 μL of 100 U/mL thrombin reconstituted in ddH_2O per mL fibrinogen. Dishes were allowed to sit for 5-minutes before being transferred to incubate at 37 °C for another 25 min utes to allow for complete gelation. After gelation, 2 mL of EGM2 per 1 mL of fibrin gel was overlaid for all gels. For conditions in which the stromal fibroblasts were cultured on top of the gel ("overlay"), DFs were introduced in the overlaid EGM2 at a concentration of 2.5×10^4 cells/mL of fibrin gel to achieve equal DF numbers per gel for both overlay and embedded conditions. For each independent experiment, multiple gels were cast for each time point. Gel constructs (0.5 mL total volume) were fabricated in 24-well tissue culture plates (Corning Inc) for bulk rheology and network quantification assays. For micro-rheology and reflection confocal imaging, gel constructs (1 mL total volume) were fabricated in 35 mm glass bottom dishes (MatTek, Ashland, MA).

For experiments involving Transwell inserts, fibrin based gel constructs (2 mL total volume) were fabricated in the bottom chamber of 6-well Transwell plates (24 mm diameter inserts containing 3.0 μm pores; Corning). DFs were cultured on top of the insert, and DAPI staining was used to confirm these cells did not migrate through the porous insert to the gel surface during the assay. Because the bottom of the insert would rest on the gel if used as provided, sterilized silicon O-rings (MSC, Melville, NY, part # S70-028) were used to space the insert off the top of the gel. All tissue constructs were cultured for up to two weeks with media exchanged on day 1 and every two days thereafter.

Fluorescent imaging and quantification of capillary morphogenesis

Images were acquired using an Olympus IX81 confocal microscope equipped with a USH-103OL mercury lamp (Olympus America, Center Valley, PA), a Hamamatsu Orca II CCD camera (Hamamatsu Photonics, Hamamatsu City, Japan), and Metamorph Premier software (Molecular Devices, Sunnyvale, CA). For visualization of tubules and cell nuclei, co-cultures were fixed with Z-Fix aqueous buffered zinc formalin fixative (Anatech, Battle Creek, MI) and stained with a rhodamine-conjugated lectin from *Ulex europaeus* (UEA, Vector Laboratories, Burlingame, CA) and 4′,6-diamidino-2-phenylindol (DAPI, Sigma-Aldrich). UEA binds glycoproteins and glycolipids specific to endothelial cells. UEA- and DAPI-stained samples were acquired using red (Ex: 562 nm, bandwidth: 40 nm; Em: 641 nm, bandwidth: 75 nm) and blue (Ex: 377 nm, bandwidth: 50 nm; Em: 477 nm, bandwidth: 60 nm) filter sets, respectively. Network length was quantified at days 1, 4, 7, and 14 with all beads imaged at 4x magnification. On day 14, multiple images often had to be stitched together to fit the entire network from a single bead. For unbiased measurements, the microscope was rastered through each gel and all beads were imaged that were far enough away from the edge of plate such that sprouting was unimpinged and did not have overlapping networks with a neighboring bead. This resulted in 8–40 beads per condition for each independent experiment being quantified, with diminishing beads meeting the criteria

as time progressed. Three independent experiments (N=3) were conducted for each condition and time point, and the aggregate data from all beads across all 3 independent experiments were presented to illustrate the spread in biological response. Total tube length per bead was quantified using the Angiogenesis Tube Formation module in Metamorph. The average network length per bead for each condition of each independent experiment was then used for statistical analysis. DF proliferation in overlay conditions was quantified by taking DAPI images of the DFs in a monolayer on top of the gel and manually determining cell density.

Bulk rheology

The bulk mechanical properties of fibrin-based constructs were measured via parallel plate shear rheology using an AR-G2 rheometer (TA Instruments, New Castle, DE) equipped with an 8 mm diameter measurement head and a Peltier stage. Oscillatory shear measurements of 6% strain amplitude and a frequency of 1 rad/sec were performed on days 1, 4, 7, and 14 directly in multi-well tissue culture plates with the rheometer stage maintained at 37 °C. Cell culture media were aspirated before measur ements, with a small volume left to ensure the gel remained wet. Rheology of elastic pre-swollen hydrogels typically involves application of a small normal force prior to data acquisition, and/or use of a consistent gap width between the bottom of the sample and the platen. However, fibrin's viscoelasticity precludes use of the former method, while varying degrees of cell-mediated gel compaction over time preclude the latter. Instead, a protocol was developed whereby the top platen was lowered until it made initial contact with the hydrogel, followed by measurements of shear modulus (G') taken at 200 μm intervals while closing the gap between platen and stage. Gels exhibited a plateau in G' as the gap was progressively decreased after making contact with the gel (Supplementary Fig. 1 A/B). The peak G' measured of 3 gap heights after making contact with the gel was used as our reported value for the given region of interest. One region of interest was interrogated per gel in 24-well plates, and three regions of interest were interrogated per gel in 6-well plates. The measurement head was carefully centered in 24-well plates to avoid edge effects contributing to G' measurements. Comparisons between acellular gels in 24 and 6-well plates over time (2.5 cm^2 and 9.8 cm^2 areas, respectively) were used to confirm the robustness of the methods across gels of different sizes (Supplementary Fig. 1C). Overlay cultures in 6-well plates were also tracked over 14 days to ensure well size did not influence observed stiffening behavior (Supplementary Fig. 2). Overlay and embedded conditions with AMR beads included were also tested to ensure bulk G' was unaffected by their inclusion (Supplementary Fig. 3). At least 3 measurements were taken per time point per independent experiment. Three independent experiments were conducted (N=3) and for each independent experiment, the gels for all time points were cast from the same stock of reagents.

Laser tweezers-based Active Microrheology

Active microrheology (AMR) was conducted using a dual-laser optical tweezers system, as has been previously described [24] and used in the study of capillary morphogenesis [14]. Briefly, fibrin hydrogels were polymerized as described above within 35 mm glass bottom dishes (MatTek, Ashland, MA) with a dispersion of 2 μm carboxylated silica microbeads (Bangs Laboratories, Fishers, IN) at a concentration of 0.08% (w/v) throughout the

hydrogel. During AMR measurements, beads within a volume of approximately 250 × 175 × 30 μm are oscillated at 50 Hz by optical forces induced by a focused 1064 nm laser (trapping beam), at an amplitude of 175 nm. A stationary 785 nm laser (detection beam) was used to detect each probe particle movement in response to the driving force. The oscillation of the input trapping beam and the deflection of the detection beam by the microbead are recorded by a pair of quadrant photodiodes (Newport, Irvine, CA). These measurements allow for calculation of the complex material response α^*. Data here is presented as the real component (G′) of the complex shear modulus G^*, computed from α^*, as previously done [25, 26]. AMR measurements were performed on days 1, 4, 7, and 14 (N=3, per day, per condition) within a custom-built stage top incubator. The volume measured within each measurement location within cell-free samples was chosen randomly, while measurements within capillary morphogenesis assays were chosen to be localized around the sprouting endothelial cells or proximal to Cytodex beads on day 1.

Confocal Reflection Microscopy

Reflection confocal stacks were acquired prior to AMR measurement of each sample. Confocal microscopy was conducted using a Fluoview 1200 system (Olympus), integrated into the optical tweezers microscope. Image stacks were imaged using the 488 nm laser line with a depth of approximately 60 μm and step size of 1 μm. For z-projections, stacks were trimmed to remove effect of glass aberration in reflection confocal and in order to keep a consistent number of planes for each z projection. Images were acquired using the same objective as for AMR; 1.45NA 60X TIRF Oil Objective (Olympus).

Statistics

Varying statistical methods were performed depending on the nature of the data analyzed and are indicated as appropriate on the figure captions. For analyzing network length, the average sprout length per bead from 8–40 beads per time point per replicate was considered for statistical analysis in comparing conditions. Linear regression was used for analyzing network length data for embedded and overlay conditions. For analyzing bulk rheology data, the average bulk modulus from 3–6 ROIs per time point per replicate was considered in comparing conditions. Heteroscedastic 2-tail t-tests were used to verify overlay and Transwell conditions had equitable sprouting on any given day, that AMR beads do not influence bulk G′ or sprouting, and that culture well size does not influence bulk-G′. One-way ANOVA was used to determine differences in bulk mechanical properties and followed with Tukey HSD post-hoc testing if differences were detected. Mann-Whitney U tests with a Bonferroni correction were performed between pairs of aggregate AMR data.

Results

DFs stimulate EC neovessel formation when overlaid or embedded in fibrin matrices

ECs cultured on microcarrier beads embedded in fibrin gels of physiological concentration [27] undergo a complex 3D morphogenetic program that results in vessel-like structures radiating from the microcarrier bead when co-cultured with a variety of stromal cells [16, 18, 28]. Here we demonstrate that normal human dermal fibroblasts (DFs), a clinically relevant and potentially autologous cell source, similarly support angiogenic outgrowth of

ECs from microcarrier beads. DFs were either embedded or overlaid on the fibrin matrix to better elucidate the relative contributions of DFs versus EC tubules on the micro- and macro-rheological properties of the gel. Cartoon schematics of these two culture models are shown (Fig. 1A), along with representative images of the typical morphogenetic progression for both culture models (Fig. 1B). (Day 1 images reveal approximately comparable levels of EC confluence on the Cytodex beads achieved via the methods described.) Quantification of these types of images over a 14-day time course reveals an increase in the total length of the vessel-like networks for both conditions, with aggregate data from all beads across each independent experiment shown to illustrate the spread in the observed biological response (Fig. 1C). The average total network lengths for the embedded culture model were consistently higher than the overlay model after day 1, but this increase was not statistically significant. Additionally, inclusion of AMR beads did not affect the rate of network formation (Supplementary Fig. 4). Over the duration of the culture period, the average network length per bead scaled across multiple orders of magnitude with the variance scaling accordingly. Data were log transformed and analyzed with a general linear model. The resulting model is: Log(Network Length) = 3.776*Log(Day). The single regression parameter is highly significant with $p < 0.0001$ and the model has an R^2 value of 0.988, demonstrating that vessel growth was exponential in time.

Acellular fibrin gels are mechanically stable over 14 days as assessed by macro-rheology and AMR

To characterize the bulk rheological properties of both acellular (pre-swollen) and cell-seeded fibrin constructs, we devised a new method described in the Supplemental Materials and Methods. Cartoon schematics illustrating the relative scale of bulk rheology compared to AMR are presented in Fig. 2A to illustrate the large difference in resolution between the two techniques. Bulk rheology showed acellular fibrin gels are mechanically stable, maintaining a nearly constant (time-invariant) G' of 119 ± 19 Pa (mean + st. dev. from all trials and days) over the course of the culture period. Moreover, the inclusion of Cytodex (Fig. 2B) and/or AMR beads (Supplementary Fig. 5) did not influence the bulk properties of the gel. Additionally, agreement between G' measurements of gels cast in multiple well sizes illustrates the validity of the method developed, independent of gel size (Supplementary Fig. 1). Moving forward, we have used G' (the elastic component of the shear modulus) interchangeably with the more colloquial term “stiffness.”

AMR measurements of acellular fibrin gels, both with and without Cytodex beads, exhibited notable stiffness heterogeneity spanning nearly two orders of magnitude (Fig. 2C; min value of 8 Pa, max value of 933 Pa across all conditions and time points shown on the graph). Repeatedly, the mean stiffness of these cell-free systems was slightly higher at Day 1, as compared to Days 4, 7, and 14 ($p<0.05$, for both +/− Cytodex beads). However, comparisons of local G' values across the later time points were not statistically different from one another, illustrating the mechanical stability of these acellular fibrin gels at the microscale consistent with bulk rheology. Furthermore, the presence of the Cytodex beads did not appreciably affect the distribution of local stiffness, as demonstrated by plotting G' values at increasing distance from the Cytodex beads (Fig. 2D). Additionally, confocal reflection

images near Cytodex beads were indistinguishable from gels without cytodex beads, illustrating that Cytodex beads do not disrupt the fibrillar architecture (Fig. 2E, F).

Bulk rheology reveals tissue constructs stiffen over time during morphogenesis

Fibrin gels with DFs either overlaid or embedded demonstrated significant stiffening over time, with overlay conditions stiffening more rapidly than embedded conditions (Fig. 3A). Controls in which DFs were included but Cytodex microcarrier beads were not coated with ECs demonstrate similar bulk stiffening behavior over time (Fig. 3B). Scaffolds with DFs embedded stiffened ~2-fold to a final G' of 253 ± 27 Pa, while scaffolds with DFs overlaid stiffened ~3.3-fold to a final G' of ~394 ± 43 Pa over the course of 2 weeks. Heteroscedastic 2-tail t-tests were used to verify no significant differences occurred between G' measured for any given culture model and day compared to its respective *DF Only* control (Fig. 3A, 3B). In addition, experiments in which DFs were cultured on Transwell inserts, and then removed for gel rheological measurements, showed that construct mechanical properties did not change significantly over a 14-day time course in the absence of DFs, even when ECs were included in the culture and tubulogenesis occurred (Fig. 3C). Lack of contact of the DFs with the fibrin construct via the Transwell did not adversely affect capillary sprouting, as revealed by the equivalent total network lengths (Fig. 3D). Together, these data demonstrate that DFs dominate the bulk stiffening of the scaffolds, while the ECs undergoing morphogenesis did not significantly affect the bulk mechanical properties of the constructs in this assay.

Capillary morphogenesis is accompanied by dynamic spatiotemporal changes in local ECM stiffness and organization

Results from selected AMR measurements for both overlay and embedded conditions proximal to the endothelial sprouts show that ECM micro-stiffness changed considerably in both space and time during capillary sprouting (Fig. 4A, 4B, **phase**). In some cases, AMR beads in close proximity reported G' values that differed by as much as 5–10x within only a few microns in the same ECM (Fig. 4, **arrows**). Matched maximum intensity confocal reflection z-projections (Fig. 4A, 4B, **confocal reflection**) demonstrated how the ECM was simultaneously remodeled. At early time points (Days 1 and 4), a typical fibrin mesh was detected proximal to the ECs. Stepping through assembled z-stacks revealed a distinct high contrast fibrillar architecture surrounding Cytodex beads on Day 1 for both the overlay (Supplementary Video 1) and embedded (Supplementary Video 2) culture models; this architecture is a hallmark signature of fibrin's microstructure. In the embedded model, however, the ECM was already changing spatially around the embedded fibroblasts. By Day 14, this fibrillar meshwork was replaced with a diffuse signal indicative of remodeling by the cells at later time points (Days 7 and 14). The fibrous structure was difficult to resolve near capillaries in the overlay conditions (Supplementary Video 3), and throughout the dish for embedded cultures (Supplementary Video 4). Interestingly, changes in pericellular ECM architecture over time did not necessarily correlate with regions of elevated stiffness as measured by AMR in the same locations. This was particularly evident in the Day 7 overlay condition, where punctate stiff areas are found both in and out of the remodeled area, though generally appears elevated near sprouts.

AMR quantitatively reveals significant local ECM stiffness heterogeneities during capillary morphogenesis

AMR measurements were conducted for both the overlay and embedded conditions in triplicate, and the results are shown in aggregate (Fig. 5A). Generally, there was an increase in average micro-stiffness over time. As early as Day 1, the embedded condition showed a broader range of G' values as compared to the overlay condition, with both conditions showing an orders-of-magnitude distribution. Within the embedded condition, this heterogeneity was observed as early as Day 1. Consistent with acellular gels (Fig. 2C), average local stiffness in the overlay condition decreased slightly between Days 1 and 4 ($p<0.05$), and by Day 14 was similar on average to the embedded condition. To assess the effects of DFs on the peri-endothelial stiffness, AMR was conducted in fibrin gels containing only fibroblasts in both the overlay and embedded conditions (Fig. 5B). In the embedded case, the effects of fibroblast remodeling were evident (increasing G') by Day 7, whereas in the overlay case, no such effect was observed. In fact, overlay gels softened at Day 14 ($p<0.05$, compared to all other days), an effect not observed with bulk rheology (Fig. 3B).

To further analyze the spatial distribution of stiffness observed in both the overlay and embedded conditions, AMR measurements were classified as either near or far, based on the proximity of each probe particle (<50μm or >50μm, respectively) to the nearest endothelial tubule (Fig. 5C). Within these conditions, G'_{near} is significantly greater than G'_{far} at all time points, except for Day 1 of the embedded case (Mann-Whitney Test, $p<0.05$). This indicates that the effects of endothelial vessel stiffening of the ECM are concentrated proximal to the vessel, with the effect dissipating with distance. Plots of G' as a function of probe bead proximity to the ECs (Fig. 5D) show that in the overlay case stiffening is concentrated in a region approximately within 50 μm of the ECs and increases over time. In contrast, the stiffness topography is more heterogeneous at all time points in the embedded case.

Discussion

Branching morphogenesis is a complex phenomenon that occurs throughout the life of all metazoan organisms [29], and there is strong evidence that ECM mechanics and cell-generated forces play important roles in shaping the organization (and disorganization) of both normal and diseased tissues [30, 31]. Studies using biomimetic materials have shown that matrix stiffness regulates cell fate in 2D [7] and 3D [9]. More recent studies have shown the ECM's mechanical regulation of cell behavior goes well beyond initial bulk material properties (e.g., compressive, tensile, shear moduli), with strong evidence that stress relaxation [32], fibrillar architectures [33], mechanical patterns/gradients [34, 35], and dynamic changes in mechanical properties [36–38] all play significant roles. To better understand the mechanical influence of a natural ECM on a complex morphogenetic process in 3D, we applied a laser tweezers-based active microrheology method and traditional parallel plate shear macrorheology to a well-established and biologically relevant 3D fibrin-based co-culture model of capillary morphogenesis, and tracked the spatiotemporal

evolution of the micro- and macro-scale shear elastic modulus during the formation of an extensive microvascular network.

AMR revealed mechanical micro-heterogeneities within acellular fibrin-based matrices, with G′ values spanning an order of magnitude within each gel. This microscale heterogeneity increased in the presence of cells and with time in culture, coincident with an overall increase in the bulk G′ values of the tissue constructs. Experiments to dissect the cellular origins of this increased stiffness revealed that the supportive DFs largely accounted for the observed increases in the bulk mechanical properties of the ECM, as DF monocultures lacking ECs also increased their bulk mechanical properties with time in culture. Additional experiments in which DFs were cultured on a Transwell insert placed on top of the gel revealed that the bulk mechanical properties of gels not in physical contact with DFs did not increase. Equivalent EC sprouting occurred when DFs were in direct contact with the gel or on a Transwell. Because we have previously shown that sprouting is deficient in the presence of fibroblast-conditioned media [13], these experiments show that reciprocal cross-talk between ECs and DFs necessary for morphogenesis still occurs when the latter are cultured on Transwells.

While the bulk mechanical property changes were largely attributable to the DFs, AMR revealed that ECs undergoing sprouting angiogenesis also progressively stiffened the ECM as they invaded. Significant increases in the micro-stiffness of the ECM occurred within 50 μm (“near”) of the sprouting vessel-like structures, regardless of whether DFs were overlaid or embedded in the matrix. The AMR experiments in the overlay conditions were particularly indicative of the EC-induced local stiffening because the DFs were located on top of the gel a fixed distance away from the z-plane (> 500 μm) in which the EC-coated beads tend to settle and in which our AMR measurements were taken. The increased heterogeneity of G′ values with time in the “near” region proximal to the vessel-like structures in the overlay conditions was also likely due to ECs. ECs apply traction forces [12, 14] and deposit new matrix [39] during capillary morphogenesis, both of which would be expected to locally stiffen the ECM.

In addition to our AMR measurements, we observed changes in ECM architecture during morphogenesis via confocal reflection microscopy. Previous studies have shown that EC tubules invading a fibrous collagen ECM deposit new collagen matrix (appearing specular as opposed to fibrillar) proximal to the lumen as EC tubules grow [39]. The ECM’s appearance proximal to vessels in our culture models (Supplementary Videos 3 and 4) was consistent with these previous findings. What has not been clear is how such changes affect local stiffness over time. Our AMR results show that local stiffness heterogeneity increased over time in culture, an effect localized to EC tubules in the overlay culture, but ubiquitous in the embedded cultures that contain an increasing population of DFs. In some cases, stiffness distal to EC tubules and located in fibrous ECM increased to values similar to those found proximal to EC tubules in specular ECM. Furthermore, this distal effect was limited in extent for the overlay conditions; beyond ~50 μm from the tubule surface, stiffness values were similar to those measured by bulk rheology and AMR of acellular gels. Therefore, areas of obvious matrix remodeling did not necessarily coincide with regions of elevated stiffness or even the greatest stiffness heterogeneities. This observation casts important

limitations on methods that correlate mechanical properties with fiber architecture [40] or rely on quantification of fiber deformations [41].

In the context of vascular morphogenesis, inconsistencies regarding the roles of ECM mechanics remain in the literature. Early evidence demonstrated that mechanical cues directly impact tubulogenesis, with softer gels better able to support capillary morphogenesis in 2D [42, 43]. In 3D cultures, angiogenic process extension was attenuated in fibrin gels whose mechanical properties were manipulated by adding exogenous factor XIII to form additional cross-links [44]. We previously demonstrated that increasing fibrin's bulk mechanical properties by increasing fibrinogen concentration beyond the physiologic provisional clot concentration used here (~2.5 mg/mL) [27] results in significant reductions in angiogenic sprouting not only *in vitro* [15] but also *in vivo* [45]; however, sub-physiologic concentrations yield overly soft gels that slowed angiogenic invasion due to reduced resistance to cell-generated traction forces [14]. Efforts to decouple ECM stiffness from other cues using glycated collagen matrices have demonstrated that stiffer ECM promotes increased angiogenic outgrowth, invasion, and branching, independent of changes in matrix density [46, 47]. Similarly, angiogenic invasion of ECs was increased in collagen gels cross-linked with transglutaminase to increase the stiffness without affecting the concentration [48]. However, other studies have reported that increased stiffness induced by collagen glycation attenuates vessel morphogenesis [49, 50].

Because of the limitations of natural ECMs and the inconsistencies in the literature, we (and many others) have turned to synthetic material platforms in an effort to decouple the mechanical and chemical effects of the ECM and thereby differentiate the contributions of mechanical cues in isolation. In such systems, softer, less cross-linked gels susceptible to cell-secreted proteases were better able to support the formation of vessel-like networks *in vitro* [51, 52]; the identity of the degradable peptides was a bigger influence than the starting mechanical properties of the gels on the formation of functional microvasculature *in vivo* [52]. However, engineered hydrogels lack key features of native ECM, which is typically fibrillar, macroporous, heterogeneous, mechanically anisotropic, and is actively remodeled by the cells that reside within it. The amorphous nature and mechanical homogeneity of synthetic gels are essential for their utility in 3D traction force microscopy [53], but questions remain regarding their physiological relevance for addressing mechanistic questions.

Our findings underscore the importance of characterizing across length scales when deciphering the roles of ECM mechanics on morphogenesis in 3D. Bulk rheology was useful for establishing ensemble averaged mechanical properties and quantifying the large degrees of stromal cell-mediated matrix remodeling with a relatively accessible technique. Understanding bulk properties is important for handling of tissue constructs and regenerative medicine applications. By contrast, AMR was useful for the precise spatiotemporal quantification of ECM mechanics on subcellular length scales during 3D capillary morphogenesis in soft fibrin matrices. Similar AMR measurements have also revealed enormous heterogeneity in the micromechanical properties of type-I collagen gels [54]. Interestingly, in these collagen gels, local cell-mediated stiffening requires both myosin-mediated traction forces [54] and active proteolysis via MMPs [55]. Future work will

address if the wide spatiotemporal variations in ECM stiffness observed during capillary growth and invasion in soft fibrin gels translate to other natural materials (of different concentrations), and if they directly influence phenotypic bifurcations (i.e., cell fate decisions), including the induction of vessel branching or the guidance of vascular invasion.

Supplementary Material

Refer to Web version on PubMed Central for supplementary material.

Acknowledgments

Research reported in this publication was supported by the National Heart, Lung, and Blood Institute of the National Institutes of Health under Award Number R01-HL085339. The content is solely the responsibility of the authors and does not necessarily represent the official views of the National Institutes of Health. BAJ was partially supported by the Tissue Engineering and Regeneration Training Program at the University of Michigan (T32-DE007057).

References

1. Discher DE, Janmey P, Wang Y-l. Tissue cells feel and respond to the stiffness of their substrate. Science. 2005; 310:1139–43. [PubMed: 16293750]
2. Engler A, Bacakova L, Newman C, Hategan A, Griffin M, Discher D. Substrate compliance versus ligand density in cell on gel responses. Biophys J. 2004; 86:617–28. [PubMed: 14695306]
3. Peyton SR, Putnam AJ. Extracellular matrix rigidity governs smooth muscle cell motility in a biphasic fashion. J Cell Physiol. 2005; 204:198–209. [PubMed: 15669099]
4. Beamish JA, Chen E, Putnam AJ. Engineered extracellular matrices with controlled mechanics modulate renal proximal tubular cell epithelialization. PLoS One. 2017; 12:e0181085. [PubMed: 28715434]
5. Khatiwala CB, Peyton SR, Putnam AJ. Intrinsic mechanical properties of the extracellular matrix affect the behavior of pre-osteoblastic MC3T3-E1 cells. Am J Physiol Cell Physiol. 2006; 290:C1640–50. [PubMed: 16407416]
6. Lo CM, Wang HB, Dembo M, Wang YL. Cell movement is guided by the rigidity of the substrate. Biophys J. 2000; 79:144–52. [PubMed: 10866943]
7. Engler AJ, Sen S, Sweeney HL, Discher DE. Matrix Elasticity Directs Stem Cell Lineage Specification. Cell. 2006; 126:677–89. [PubMed: 16923388]
8. Khatiwala CB, Kim PD, Peyton SR, Putnam AJ. ECM compliance regulates osteogenesis by influencing MAPK signaling downstream of RhoA and ROCK. J Bone Miner Res. 2009; 24:886–98. [PubMed: 19113908]
9. Huebsch N, Arany PR, Mao AS, Shvartsman D, Ali OA, Bencherif SA, et al. Harnessing traction-mediated manipulation of the cell/matrix interface to control stem-cell fate. Nat Mater. 2010; 9:518–26. [PubMed: 20418863]
10. Peyton SR, Kim PD, Ghajar CM, Seliktar D, Putnam AJ. The effects of matrix stiffness and RhoA on the phenotypic plasticity of smooth muscle cells in a 3-D biosynthetic hydrogel system. Biomaterials. 2008; 29:2597–607. [PubMed: 18342366]
11. Ingber DE. Mechanical signaling and the cellular response to extracellular matrix in angiogenesis and cardiovascular physiology. Circ Res. 2002; 91:877–87. [PubMed: 12433832]
12. Korff T, Augustin HG. Tensional forces in fibrillar extracellular matrices control directional capillary sprouting. J Cell Sci. 1999; 112(Pt 19):3249–58. [PubMed: 10504330]
13. Kniazeva E, Putnam AJ. Endothelial cell traction and ECM density influence both capillary morphogenesis and maintenance in 3-D. AJP: Cell Physiology. 2009; 297:C179–C87. [PubMed: 19439531]

14. Kniazeva E, Weidling JW, Singh R, Botvinick EL, Digman MA, Gratton E, et al. Quantification of local matrix deformations and mechanical properties during capillary morphogenesis in 3D. Integrative Biology. 2012; 4:431. [PubMed: 22281872]
15. Ghajar CM, Blevins KS, Hughes CC, George SC, Putnam AJ. Mesenchymal stem cells enhance angiogenesis in mechanically viable prevascularized tissues via early matrix metalloproteinase upregulation. Tissue engineering. 2006; 12:2875–88. [PubMed: 17518656]
16. Nehls V, Drenckhahn D. A Novel, Microcarrier-Based in Vitro Assay for Rapid and Reliable Quantification of Three-Dimensional Cell Migration and Angiogenesis. Microvascular Research. 1995; 50:311–22. [PubMed: 8583947]
17. Tonnesen MG, Feng X, Clark RAF. Angiogenesis in Wound Healing. Journal of Investigative Dermatology Symposium Proceedings. 2000; 5:40–6.
18. Ghajar CM, Kachgal S, Kniazeva E, Mori H, Costes SV, George SC, et al. Mesenchymal cells stimulate capillary morphogenesis via distinct proteolytic mechanisms. Experimental Cell Research. 2010; 316:813–25. [PubMed: 20067788]
19. Nakatsu MN, Sainson RCA, Aoto JN, Taylor KL, Aitkenhead M, Pérez-del-Pulgar S, et al. Angiogenic sprouting and capillary lumen formation modeled by human umbilical vein endothelial cells (HUVEC) in fibrin gels: the role of fibroblasts and Angiopoietin-1. Microvascular Research. 2003; 66:102–12. [PubMed: 12935768]
20. Newman AC, Nakatsu MN, Chou W, Gershon PD, Hughes CC. The requirement for fibroblasts in angiogenesis: fibroblast-derived matrix proteins are essential for endothelial cell lumen formation. Molecular biology of the cell. 2011; 22:3791–800. [PubMed: 21865599]
21. Tomasek JJ, Gabbiani G, Hinz B, Chaponnier C, Brown RA. Myofibroblasts and mechano-regulation of connective tissue remodelling. Nat Rev Mol Cell Biol. 2002; 3:349–63. [PubMed: 11988769]
22. Jansen Karin A, Bacabac Rommel G, Piechocka Izabela K, Koenderink Gijsje H. Cells Actively Stiffen Fibrin Networks by Generating Contractile Stress. Biophysical Journal. 2013; 105:2240–51. [PubMed: 24268136]
23. Ghajar CM, Chen X, Harris JW, Suresh V, Hughes CC, Jeon NL, et al. The effect of matrix density on the regulation of 3-D capillary morphogenesis. Biophys J. 2008; 94:1930–41. [PubMed: 17993494]
24. Kotlarchyk MA, Shreim SG, Alvarez-Elizondo MB, Estrada LC, Singh R, Valdevit L, et al. Concentration Independent Modulation of Local Micromechanics in a Fibrin Gel. PLoS ONE. 2011; 6:e20201. [PubMed: 21629793]
25. Brau RR, Ferrer JM, Lee H, Castro CE, Tam BK, Tarsa PB, et al. Passive and active microrheology with optical tweezers. Journal of Optics A: Pure and Applied Optics. 2007; 9:S103.
26. Mizuno D, Head DA, MacKintosh FC, Schmidt CF. Active and Passive Microrheology in Equilibrium and Nonequilibrium Systems. Macromolecules. 2008; 41:7194–202.
27. Weisel JW. Biophysics. Enigmas of blood clot elasticity. Science. 2008; 320:456–7. [PubMed: 18436761]
28. Kachgal S, Putnam AJ. Mesenchymal stem cells from adipose and bone marrow promote angiogenesis via distinct cytokine and protease expression mechanisms. Angiogenesis. 2011; 14:47–59. [PubMed: 21104120]
29. Lu P, Werb Z. Patterning mechanisms of branched organs. Science. 2008; 322:1506–9. [PubMed: 19056977]
30. Bellas E, Chen CS. Forms, forces, and stem cell fate. Curr Opin Cell Biol. 2014; 31:92–7. [PubMed: 25269668]
31. Mammoto T, Mammoto A, Ingber DE. Mechanobiology and developmental control. Annu Rev Cell Dev Biol. 2013; 29:27–61. [PubMed: 24099083]
32. Chaudhuri O, Gu L, Klumpers D, Darnell M, Bencherif SA, Weaver JC, et al. Hydrogels with tunable stress relaxation regulate stem cell fate and activity. Nat Mater. 2015
33. Baker BM, Trappmann B, Wang WY, Sakar MS, Kim IL, Shenoy VB, et al. Cell-mediated fibre recruitment drives extracellular matrix mechanosensing in engineered fibrillar microenvironments. Nat Mater. 2015; 14:1262–8. [PubMed: 26461445]

34. Tse JR, Engler AJ. Stiffness gradients mimicking in vivo tissue variation regulate mesenchymal stem cell fate. PLoS One. 2011; 6:e15978. [PubMed: 21246050]
35. Yang C, DelRio FW, Ma H, Killaars AR, Basta LP, Kyburz KA, et al. Spatially patterned matrix elasticity directs stem cell fate. Proc Natl Acad Sci U S A. 2016; 113:E4439–45. [PubMed: 27436901]
36. Khetan S, Guvendiren M, Legant WR, Cohen DM, Chen CS, Burdick JA. Degradation-mediated cellular traction directs stem cell fate in covalently crosslinked three-dimensional hydrogels. Nature materials. 2013; 12:458–65. [PubMed: 23524375]
37. Yang C, Tibbitt MW, Basta L, Anseth KS. Mechanical memory and dosing influence stem cell fate. Nat Mater. 2014; 13:645–52. [PubMed: 24633344]
38. Lee J, Abdeen AA, Kilian KA. Rewiring mesenchymal stem cell lineage specification by switching the biophysical microenvironment. Sci Rep. 2014; 4:5188. [PubMed: 24898422]
39. Lee PF, Yeh AT, Bayless KJ. Nonlinear optical microscopy reveals invading endothelial cells anisotropically alter three-dimensional collagen matrices. Experimental cell research. 2009; 315:396–410. [PubMed: 19041305]
40. Raub CB, Suresh V, Krasieva T, Lyubovitsky J, Mih JD, Putnam AJ, et al. Noninvasive assessment of collagen gel microstructure and mechanics using multiphoton microscopy. Biophys J. 2007; 92:2212–22. [PubMed: 17172303]
41. Steinwachs J, Metzner C, Skodzek K, Lang N, Thievessen I, Mark C, et al. Three-dimensional force microscopy of cells in biopolymer networks. Nat Methods. 2016; 13:171–6. [PubMed: 26641311]
42. Vailhe B, Lecomte M, Wiernsperger N, Tranqui L. The formation of tubular structures by endothelial cells is under the control of fibrinolysis and mechanical factors. Angiogenesis. 1998; 2:331–44. [PubMed: 14517453]
43. Deroanne CF, Lapiere CM, Nusgens BV. In vitro tubulogenesis of endothelial cells by relaxation of the coupling extracellular matrix-cytoskeleton. Cardiovasc Res. 2001; 49:647–58. [PubMed: 11166278]
44. Urech L, Bittermann AG, Hubbell JA, Hall H. Mechanical properties, proteolytic degradability and biological modifications affect angiogenic process extension into native and modified fibrin matrices in vitro. Biomaterials. 2005; 26:1369–79. [PubMed: 15482824]
45. Kniazeva E, Kachgal S, Putnam AJ. Effects of extracellular matrix density and mesenchymal stem cells on neovascularization in vivo. Tissue Eng Part A. 2011; 17:905–14. [PubMed: 20979533]
46. Mason BN, Starchenko A, Williams RM, Bonassar LJ, Reinhart-King CA. Tuning three-dimensional collagen matrix stiffness independently of collagen concentration modulates endothelial cell behavior. Acta Biomater. 2013; 9:4635–44. [PubMed: 22902816]
47. Bordeleau F, Mason BN, Lollis EM, Mazzola M, Zanotelli MR, Somasegar S, et al. Matrix stiffening promotes a tumor vasculature phenotype. Proceedings of the National Academy of Sciences of the United States of America. 2017; 114:492–7. [PubMed: 28034921]
48. Lee P-F, Bai Y, Smith RL, Bayless KJ, Yeh AT. Angiogenic responses are enhanced in mechanically and microscopically characterized, microbial transglutaminase crosslinked collagen matrices with increased stiffness. Acta Biomaterialia. 2013; 9:7178–90. [PubMed: 23571003]
49. Francis-Sedlak ME, Moya ML, Huang JJ, Lucas SA, Chandrasekharan N, Larson JC, et al. Collagen glycation alters neovascularization in vitro and in vivo. Microvasc Res. 2010; 80:3–9. [PubMed: 20053366]
50. Kuzuya M, Satake S, Ai S, Asai T, Kanda S, Ramos MA, et al. Inhibition of angiogenesis on glycated collagen lattices. Diabetologia. 1998; 41:491–9. [PubMed: 9628264]
51. Singh RK, Seliktar D, Putnam AJ. Capillary morphogenesis in PEG-collagen hydrogels. Biomaterials. 2013; 34:9331–40. [PubMed: 24021759]
52. Vigen M, Ceccarelli J, Putnam AJ. Protease-sensitive PEG hydrogels regulate vascularization in vitro and in vivo. Macromol Biosci. 2014; 14:1368–79. [PubMed: 24943402]
53. Legant WR, Miller JS, Blakely BL, Cohen DM, Genin GM, Chen CS. Measurement of mechanical tractions exerted by cells in three-dimensional matrices. Nat Methods. 2010; 7:969–71. [PubMed: 21076420]

54. Keating M, Kurup A, Alvarez-Elizondo M, Levine AJ, Botvinick E. Spatial distributions of pericellular stiffness in natural extracellular matrices are dependent on cell-mediated proteolysis and contractility. Acta Biomater. 2017; 57:304–12. [PubMed: 28483696]

55. Tang Y, Rowe RG, Botvinick EL, Kurup A, Putnam AJ, Seiki M, et al. MT1-MMP-dependent control of skeletal stem cell commitment via a beta1-integrin/YAP/TAZ signaling axis. Dev Cell. 2013; 25:402–16. [PubMed: 23685250]

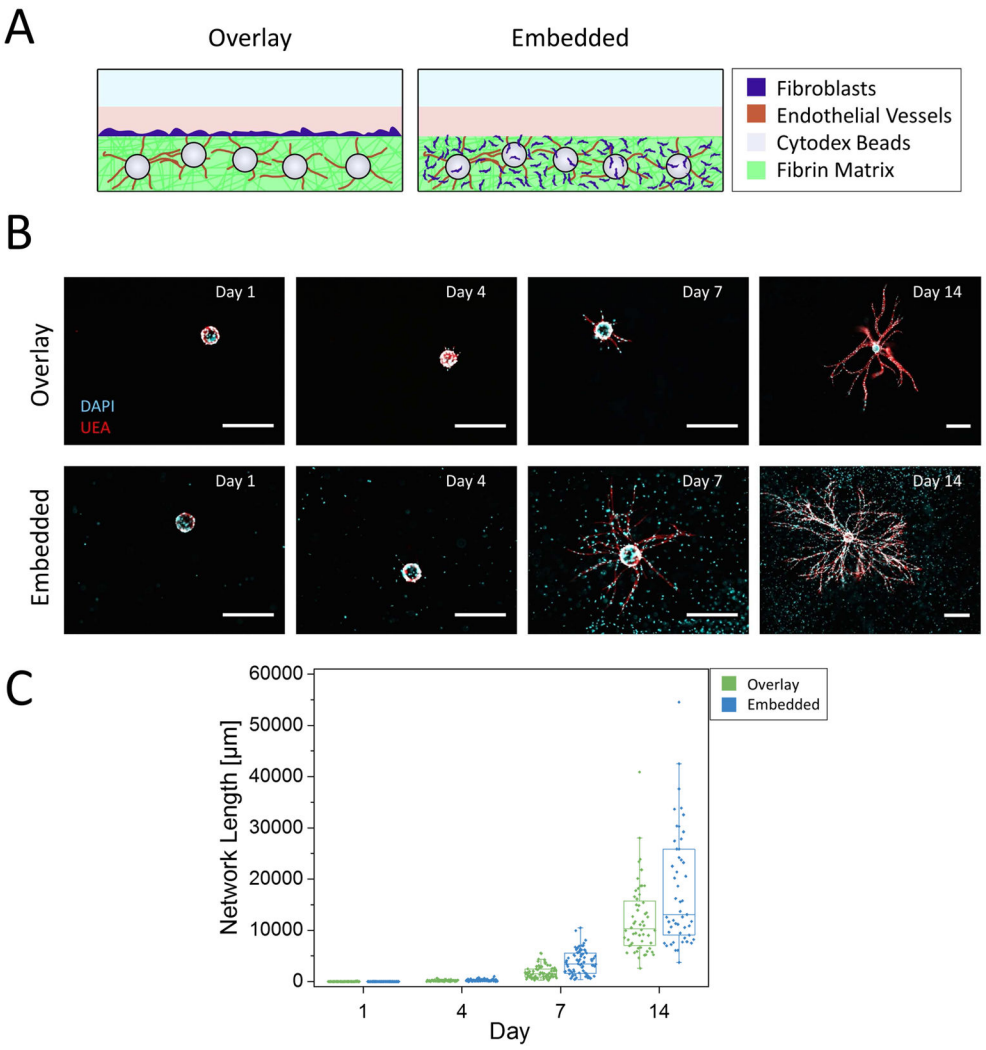

Figure 1. DFs induce EC branching morphogenesis when overlaid or embedded within 3D fibrin matrices

A) Schematic representation of the capillary morphogenesis assay. The "Overlay" condition involves culturing DFs on top of the fibrin gel, while the DFs are distributed throughout the fibrin gel in the "Embedded" condition. **B)** Representative images from each condition over a 14 day time course. UEA and DAPI staining indicate ECs and total cell nuclei, respectively. Scale bar = 500 μm. **C)** Quantified network lengths vs. time for both Overlay and Embedded conditions (8–40 beads assessed per replicate, N=3 per condition, per time point). A general linear model resulted in Log(Network Length) = 3.776*Log(Day), $p < 0.0001$, $R^2 = 0.988$. Boxed regions show median and interquartile range (IQR) of aggregate data, whiskers show range within 1.5 IQR.

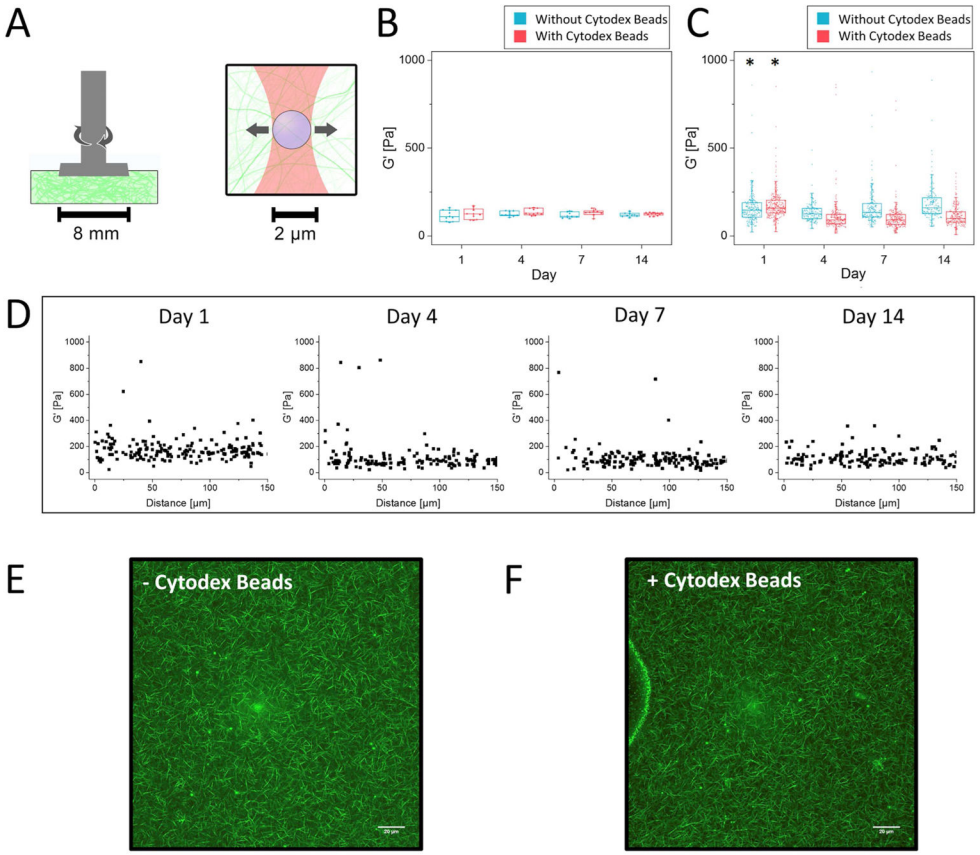

Figure 2. Bulk rheology and AMR of acellular fibrin gels reveal the gels are mechanically stable over 2 weeks in culture conditions

A) Schematic diagram of methods used to quantify stiffness in bulk using parallel plate rheology (left) and at the microscale using active microrheology (right). **B)** Bulk rheology over 14 days with (red) and without (blue) Cytodex beads. (N=3, per condition, per timepoint). One-way ANOVA of G′ +/− Cytodex beads yielded a P value of 0.93. **C)** Microrheology over 14 days with and without Cytodex beads (aggregate data, N=3 independent samples, with $n_{AMRbeads}$>150 per time point, per condition). Boxed regions in panels B and C show median and interquartile range (IQR) of aggregate data, whiskers show range within 1.5 IQR. The asterisk above Day 1 indicates significant differences ($p<0.05$) relative to all other time points for both conditions (+/− Cytodex beads). **D)** Microrheology data from **(C)** plotted as a function of distance from the edge of the Cytodex bead. **E,F)** Confocal reflection of the fibrin meshwork without and with Cytodex beads (Scale bar = 20 μm).

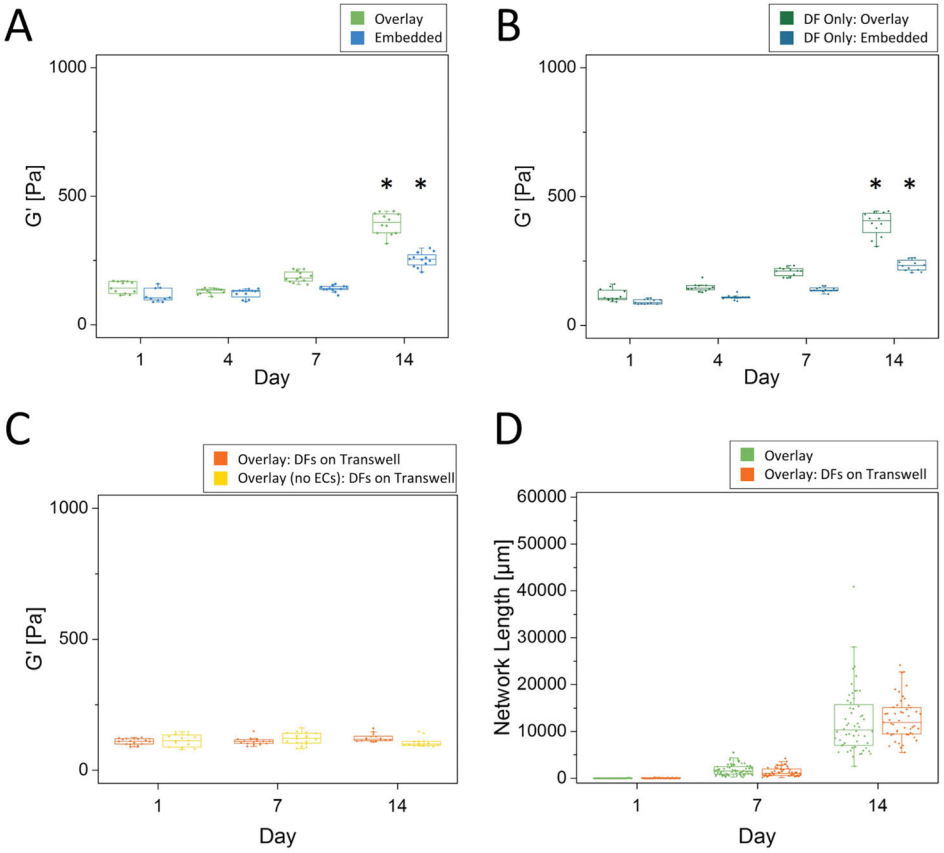

Figure 3. Bulk rheology reveals an increase in stiffness with time during morphogenesis

Parallel plate rheology of **(A)** bead assay in both the Overlay and Embedded conditions, (**B)** fibrin constructs with only DFs (no ECs) either overlaid on top of the gel or embedded within, and **(C)** a bead assay and a fibrin construct with DFs located on a Transwell (N=3 independent experiments for each time point and condition). Asterisks in **(A)** and **(B)** indicate statistical differences from all other time points for a given assay type ($p<0.05$). **D)** Quantified network lengths between the Overlay condition and Overlay with DFs on a Transwell (multiple ROIs assessed per sample, N=3, per condition, per time point). There were no statistical differences between Transwell and Overlay conditions for any given day. Boxed regions show median and interquartile range (IQR) of aggregate data, whiskers show range within 1.5 IQR.

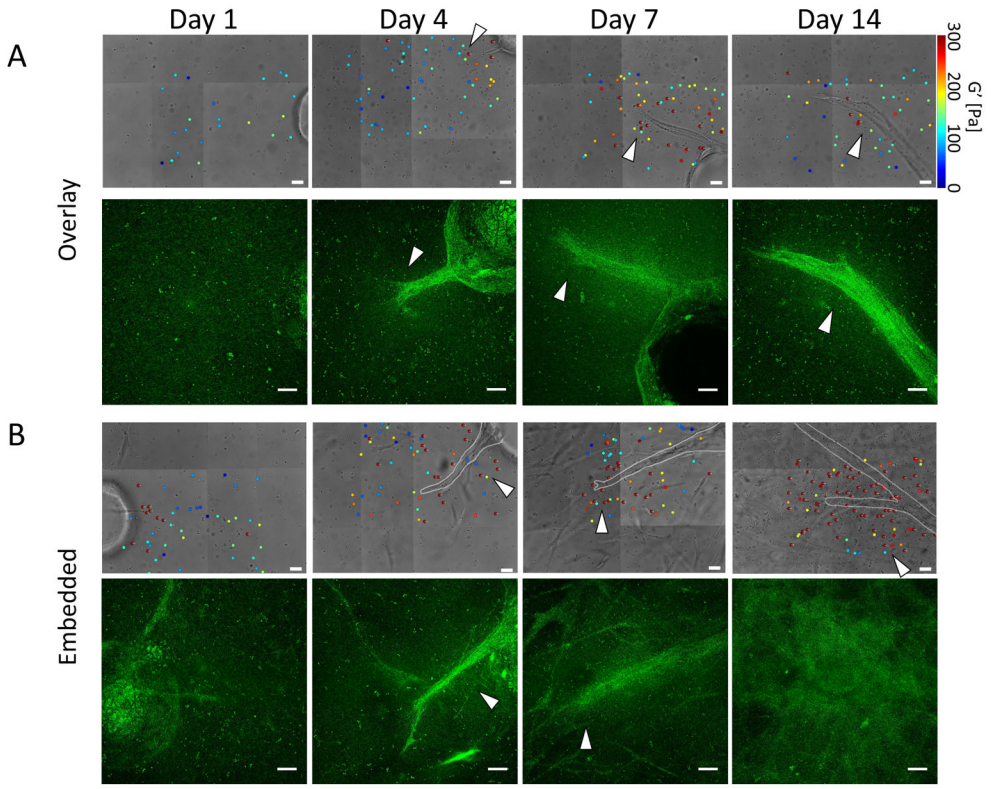

Figure 4. Capillary morphogenesis is accompanied by dynamic spatiotemporal changes in local ECM stiffness and organization

Selected stiffness maps generated using AMR and corresponding confocal reflection maximum intensity z-projections for the **(A)** Overlay and **(B)** Embedded conditions. Z-projections were created from 60 μm z-stacks with a step size of 1 μm, with those planes affected by distortion from the coverglass trimmed out prior to z-projection. Scale bar = 20 μm for brightfield images and 20 μm for reflection confocal z-projections. Arrows added emphasize areas where there is close proximity of stiffness heterogeneity, especially in the context of areas that appear different from the fibrous structure of fibrin. Please note the color map for G′ saturates at 300 Pa. Stiffness values for individual beads reporting stiffness above 300 Pa are annotated on the beads.

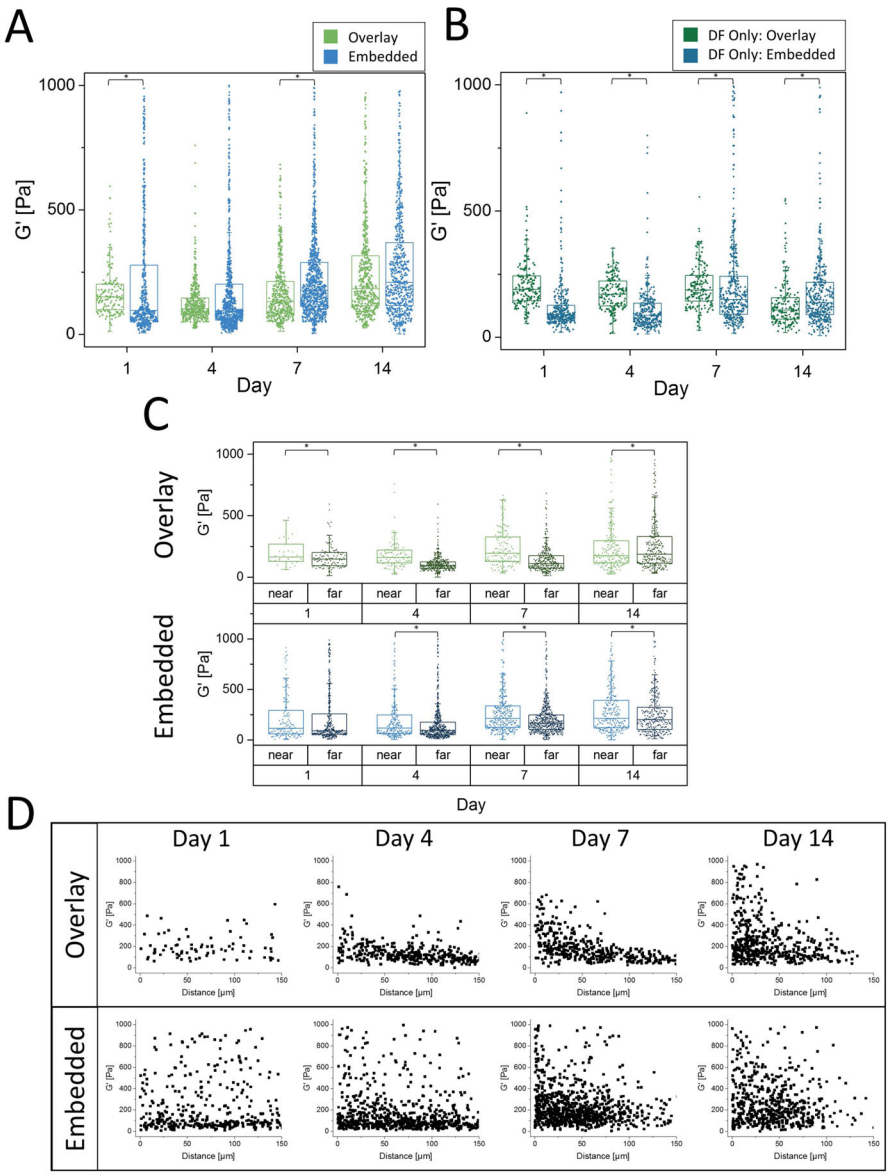

Figure 5. AMR quantitatively reveals significant local ECM stiffness heterogeneities during capillary morphogenesis

A) Microrheology proximal to the sprout tips in both the Overlay and Embedded conditions (aggregate data, N=3 per condition, per timepoint). **B)** Microrheology in fibrin constructs only containing DFs (no ECs) either overlaid on top of the gel or embedded within (aggregate data, N=3 independent samples, with $n_{AMRbeads}$>150 per time point, per condition). **C)** Microrheology from (**A**) segregated into two classes, near or far, based on distance from endothelial cells (<50 μm or >50 μm, respectively). For panels A–C, asterisks indicate statistical differences between groups ($p<0.05$) Boxed regions show median and interquartile range (IQR) of aggregate data, whiskers show range within 1.5 IQR. **D)** Microrheology data from (A) plotted as a function of probe bead proximity to the ECs.